

# Exotic atom pairs: Repulsively bound states in an optical lattice

J. HECKER DENSCHLAG

*Institut für Experimentalphysik, Universität Innsbruck, 6020 Innsbruck, Austria*

A. J. DALEY

*Institut für Theoretische Physik, Universität Innsbruck, 6020 Innsbruck, Austria*

## 1. – Introduction

Ultracold atoms in 3D optical lattices provide an intriguing environment to study strongly correlated condensed matter systems and quantum information. Unique features of these atomic many body systems include the complete control of system parameters, and - in particular contrast to solid state physics - weak couplings to dissipative environments. This so-called quantum lattice gas [1, 2] is described by a Bose or Fermi Hubbard Hamiltonian. The high control over the atoms opens the possibility to engineer a wide class of interesting many body quantum states. Seminal experiments have already demonstrated the superfluid-Mott insulator transition [3], the realisation of 1D quantum liquids with atomic gases [4, 5] (see also [6, 7]), and a Bose spin glass [8]. Here we review another recent experiment [9] where we have observed a novel kind of bound state of two atoms which is based on repulsive interactions between the particles. These repulsively bound pairs exhibit long lifetimes, even under conditions when they collide with one another. Stable repulsively bound objects should be viewed as a general phenomenon and their existence will be ubiquitous in cold atoms lattice physics. Although the experiment described here is based on bosonic  $^{87}\text{Rb}$  atoms, other composites with fermions [10] or Bose-Fermi mixtures [11] should exist in an analogous manner. Furthermore, repulsively bound objects could also be formed with more than two particles.

In the following we will first explain the theoretical background of repulsively atom pairs. Afterwards we will present the experiments which demonstrate several key properties of the pairs. Finally we give a short discussion of how these repulsively bound pairs relate to bound states in some other physical systems.

## 2. – Repulsively bound pairs

Optical lattices are generated by pairs of counterpropagating laser beams, where the resulting standing wave intensity pattern forms a periodic array of microtraps for the cold atoms, with period given by half the wavelength of the light,  $\lambda/2$ . This periodicity of the potential gives rise to a bandstructure for the atom dynamics with Bloch bands separated by band gaps, which can be controlled via the laser parameters and configuration, as shown in Fig. 1. The dynamics of an atomic Bose-Einstein condensate loaded into the lowest band of a sufficiently deep optical lattice [1, 2] is well described by a single band Bose Hubbard model [12] with Hamiltonian

$$(1) \quad \hat{H} = -J \sum_{\langle ij \rangle} \hat{b}_i^\dagger \hat{b}_j + \frac{U}{2} \sum_j \hat{b}_j^\dagger \hat{b}_j (\hat{b}_j^\dagger \hat{b}_j - 1) + \sum_i \epsilon_i \hat{b}_i^\dagger \hat{b}_i.$$

Here  $\hat{b}_i$  ( $\hat{b}_i^\dagger$ ) are destruction (creation) operators for the bosonic atoms at site  $i$ .  $J/\hbar$  and  $U$  denote respectively the tunnelling rate of atoms between neighbouring sites, and the collisional energy shift from interactions between atoms on the same site. The resulting width of the Bloch band is  $4J$ , and this single band model is valid because the kinetic energy and interaction energy in this system are much smaller than the separation of the Bloch bands  $\omega$ .

The Bose-Hubbard Hamiltonian (1) predicts the existence of stable repulsively bound atom pairs. These are most intuitively understood in the limit of strong repulsive interaction  $U \gg J$  (where  $U > 0$  but this energy is still smaller than the separation to the first excited Bloch band,  $U \ll \omega$ ). If a state is prepared with two atoms occupying a single site,  $|2_i\rangle \equiv (\hat{b}_i^\dagger)^2 |\text{vac}\rangle / \sqrt{2}$ , then it will have a potential energy offset  $\approx U$  with respect to states where the atoms are separated [see Fig. 2(left)]. This state will be unable to decay by converting the potential energy into kinetic energy, as the Bloch band provides a maximum kinetic energy for two atoms both at the edge of the Brillouin zone given by  $8J \ll U$ . Instead, the atoms will remain together, and tunnel through the lattice as a bound composite object – a repulsively bound pair.

We can observe this nature of repulsive binding in the experiment [see Fig. 2(right)]. After production of the atom pairs, as is discussed in detail in section 5, we allow the atoms to tunnel through the lattice along one dimension. If the on-site interaction of the atoms is tuned to zero with the help of a Feshbach resonance, the pairs break up within a few ms, corresponding to the tunneling timescale. However, if the effective interaction between the atoms is repulsive, we observe a remarkably long lifetime of  $t = 700$  ms (determined by an exponential fit). This lifetime is mainly limited by inelastic scattering of lattice photons.

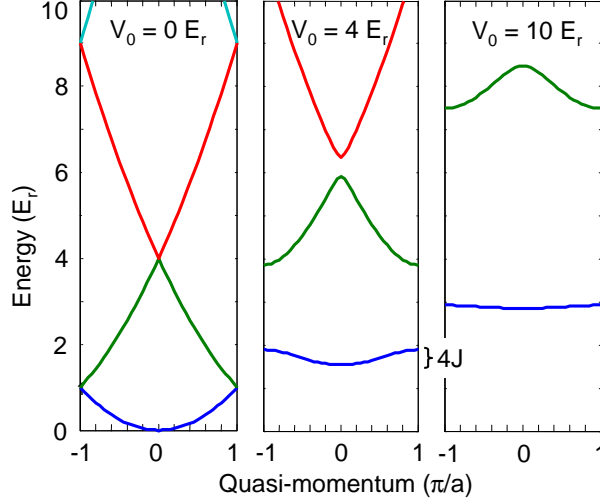


Fig. 1. – Energy spectrum for a single particle in a 1D lattice for three different potential depths  $V_0$ . The band width of the lowest Bloch band is given by  $4J$  where  $J$  is the hopping energy.  $a$  is the lattice period and  $E_r = \pi^2 \hbar^2 / 2ma^2$  denotes the recoil energy.

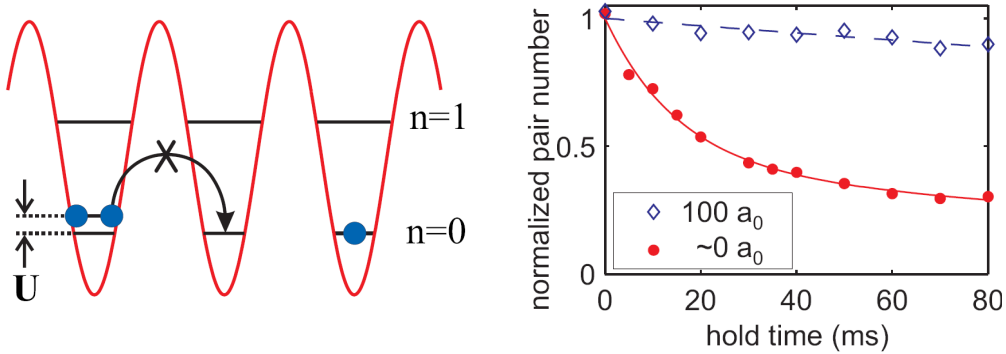


Fig. 2. – **left** A state with two atoms located on the same site of an optical lattice has an energy offset  $\approx U$  with respect to states where the atoms are separated. Breaking up of the pair is suppressed due to the lattice band structure and energy conservation, so that the pair remains bound as a composite object, which can tunnel through the lattice. In the figure,  $n = 0$  denotes the lowest Bloch band and  $n = 1$  the first excited band. **right** Breaking up of atom pairs in a shallow 3D optical lattice. [The potential depth is  $(10 \pm 0.5) E_r$  in one direction and  $(35 \pm 1.5) E_r$  in the perpendicular directions.] Shown is the remaining fraction of pairs for a scattering length of  $100 a_0$  (open diamonds) and a scattering length of about  $(0 \pm 10) a_0$  (filled circles) as a function of the hold time. The atom pairs quickly break up within a few ms if they do not interact, but stay together for a long time in case of repulsive interaction. The lines are fit curves of an exponential (dashed line) and the sum of two exponentials (solid line).

### 3. – Analytical solution of two particle problem in an optical lattice

**3.1. General Discussion.** – Our understanding of these stable pairs can be made more formal by an exact solution of the two particle Lippmann-Schwinger scattering equation on the lattice corresponding to the Bose-Hubbard Hamiltonian Eq. (1).

Denoting the primitive lattice vectors in each of the  $d$  dimensions by  $\mathbf{e}_i$ , we can write the position of the two atoms by  $\mathbf{x} = \sum_{i=1}^d x_i \mathbf{e}_i$  and  $\mathbf{y} = \sum_{i=1}^d y_i \mathbf{e}_i$ , where  $x_i, y_i$  are integers, and we can write the two atom wave function in the form  $\Psi(\mathbf{x}, \mathbf{y})$ . The related Schrödinger equation from the Bose-Hubbard model [Eq. (1)] with homogeneous background,  $\epsilon_i = 0$  then takes the form

$$(2) \quad \left[ -J \left( \tilde{\Delta}_{\mathbf{x}} + \tilde{\Delta}_{\mathbf{y}} \right) + U \delta_{\mathbf{x}, \mathbf{y}} \right] \Psi(\mathbf{x}, \mathbf{y}) = E \Psi(\mathbf{x}, \mathbf{y}),$$

where the operator

$$(3) \quad \tilde{\Delta}_{\mathbf{x}} \Psi(\mathbf{x}, \mathbf{y}) = \sum_{i=1}^d [\Psi(\mathbf{x} + \mathbf{e}_i, \mathbf{y}) + \Psi(\mathbf{x} - \mathbf{e}_i, \mathbf{y}) - 2\Psi(\mathbf{x}, \mathbf{y})]$$

denotes a discrete lattice Laplacian on a cubic lattice. Note that in order to express this in terms of the discrete lattice Laplacian we have added  $4dJ\Psi(\mathbf{x}, \mathbf{y})$  to each side of the Schrödinger equation. This effectively changes the zero of energy, so that  $E \rightarrow E + 4Jd$ . We then introduce relative coordinates  $\mathbf{r} = \mathbf{x} - \mathbf{y}$  existing on the same lattice structure as the co-ordinate  $\mathbf{x}$ , and center of mass coordinates  $\mathbf{R} = (\mathbf{x} + \mathbf{y})/2$ , existing on a lattice with the same symmetry as the original lattice but smaller lattice constant  $a/2$ . We then separate the wavefunction using the ansatz

$$(4) \quad \Psi(\mathbf{x}, \mathbf{y}) = \exp(i\mathbf{K}\mathbf{R})\psi_{\mathbf{K}}(\mathbf{r}),$$

with  $\mathbf{K}$  the centre of mass quasi-momentum. This allows us to reduce the Schrödinger equation to a single particle problem in the relative coordinate,

$$(5) \quad \left[ -2J\tilde{\Delta}_{\mathbf{r}}^{\mathbf{K}} + E_{\mathbf{K}} + U\delta_{\mathbf{r},0} \right] \psi_{\mathbf{K}}(\mathbf{r}) = E\psi_{\mathbf{K}}(\mathbf{r})$$

where  $E_{\mathbf{K}} = 4J\sum_{i=1}^d [1 - \cos(\mathbf{K}\mathbf{e}_i/2)]$  is the kinetic energy of the center of mass motion, and where the discrete lattice Laplacian for a square lattice is now given by

$$(6) \quad \tilde{\Delta}_{\mathbf{r}}^{\mathbf{K}} \Psi(\mathbf{r}) = \sum_{i=1}^d \cos(\mathbf{K}\mathbf{e}_i/2) [\Psi(\mathbf{r} + \mathbf{e}_i) + \Psi(\mathbf{r} - \mathbf{e}_i) - 2\Psi(\mathbf{r})].$$

The solutions of this Schrödinger equation can be found using the Greens function of the non-interacting problem with  $U = 0$ , which is defined by

$$(7) \quad [E - H_0] G_{\mathbf{K}}(E, \mathbf{r}) = \delta_{\mathbf{r},0},$$

with  $\delta_{\mathbf{r},0}$  a three-dimensional Kronecker delta, and  $H_0 = -2J\Delta_{\mathbf{r}}^{\mathbf{K}}$  the Hamiltonian of the non-interacting system. This equation can be easily solved via Fourier transformation,  $G(E, \mathbf{r}) = [1/(2\pi)^d] \int d^d k \tilde{G}(E, \mathbf{k}) \exp(i\mathbf{k}\mathbf{r})$ , and we obtain the solution

$$(8) \quad \tilde{G}_{\mathbf{K}}(E, \mathbf{k}) = \frac{1}{E - \epsilon_{\mathbf{K}}(\mathbf{k}) + i\eta},$$

where  $\epsilon_{\mathbf{K}}(\mathbf{k})$  accounts for the dispersion relation of the non-interacting system,

$$(9) \quad \epsilon_{\mathbf{K}}(\mathbf{k}) = 4J \sum_{i=1}^d \cos \frac{K_i a}{2} [1 - \cos(k_i a)].$$

The solutions of Eq. (5) can be divided into two classes: scattering states, and bound (localised) states. We will first analyze the scattering states.

**3.2. Scattering States.** – Similarly to scattering problems involving particles in free space, the scattering states of particles on the lattice with energy  $E$  obey the Lippmann-Schwinger equation

$$(10) \quad \psi_E(\mathbf{r}) = \psi_E^0(\mathbf{r}) + \sum_{\mathbf{r}'} G_{\mathbf{K}}(E, \mathbf{r} - \mathbf{r}') V(\mathbf{r}') \psi_E(\mathbf{r}')$$

with  $\psi_E^0 = \exp(i\mathbf{k}\mathbf{r})$  an eigenstate of  $H_0$  with energy  $E = \epsilon_{\mathbf{K}}(\mathbf{k})$ . In the present situation with a short range potential  $V(\mathbf{r}) = U\delta_{\mathbf{r},0}$ , the Lippmann-Schwinger equation can be solved via a resummation of the Born expansion and we obtain

$$(11) \quad \psi_E(\mathbf{r}) = \exp(i\mathbf{k}\mathbf{r}) - 8\pi J f_E(\mathbf{K}) G_{\mathbf{K}}(E, \mathbf{r})$$

with scattering amplitude

$$(12) \quad f_E(\mathbf{K}) = -\frac{1}{4\pi} \frac{U/(2J)}{1 - G_{\mathbf{K}}(E, 0)U},$$

where the total energy is  $E = \epsilon_{\mathbf{k}, \mathbf{K}} + E_{\mathbf{K}}$ ,  $\epsilon_{\mathbf{k}, \mathbf{K}} = 4J \sum_{i=1}^d \cos(\mathbf{K}\mathbf{e}_i/2) [1 - \cos(\mathbf{k}\mathbf{e}_i)]$ , and

$$(13) \quad G_{\mathbf{K}}(E, 0) = \frac{4\pi}{2J} \int \frac{d\mathbf{k}}{(2\pi)^d} \frac{1}{E/(2J) - 2 \sum_{i=1}^d \cos \frac{K_i a}{2} (1 - \cos k_i a)}.$$

The scattering states  $\psi_E(\mathbf{r})$  correspond to two free atoms moving on the lattice and undergoing scattering processes. The corresponding energies appear as a continuum in Fig. 3. In order to make a connection to the scattering length in free space, we can consider the limit of small momenta of the incoming plane wave, i.e.,  $\mathbf{k} \rightarrow 0$ ,  $\mathbf{K} \rightarrow 0$  and  $E \rightarrow 0$ . Then the solution (11) reduces in the limit  $\mathbf{r} \rightarrow \infty$  to

$$(14) \quad \psi_E(\mathbf{r}) \sim \psi_E^0(\mathbf{r}) + f(\mathbf{k}, \mathbf{k}') \frac{\exp(ikr)}{r}$$

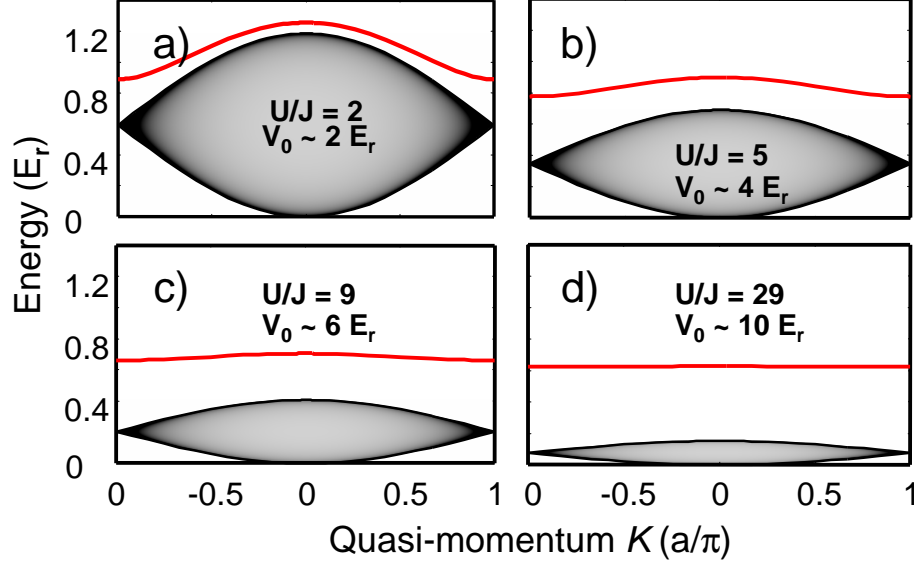


Fig. 3. – Two particle energy spectrum in a 1D lattice for four different potential depths  $V_0$  as a function of centre of mass quasi-momentum  $K$ . The Bloch band for repulsively bound pairs is located above the continuum of unbound scattering states. The grey level for the shading of the continuum is proportional to the density of states.

with the scattering amplitude

$$(15) \quad f(\mathbf{k}, \mathbf{k}') = -a_s = -\frac{1}{4\pi} \frac{U/(2J)}{1 - \alpha U/(2J)},$$

equivalent to the  $s$ -wave scattering length  $a_s$ , while the constant  $\alpha = \lim_{E \rightarrow 0} G(E, 0)$  is  $\alpha \approx -0.25$  [13].

**3.3. Bound States.** – Note that the scattering amplitude in Eq. (11) contains a pole, associated with a bound state. We now focus on these bound states in the regime,  $U > 0$ , which will correspond to a repulsively bound pair. First we note that we can write Eq. (7) in the form

$$(16) \quad [E - H_0] G_{\mathbf{K}}(E, \mathbf{r}) = \frac{1}{G_{\mathbf{K}}(E, 0)} \delta_{\mathbf{r}, 0} G_{\mathbf{K}}(E, \mathbf{r}).$$

As a consequence, the function  $\psi_{\mathbf{K}}^{\text{BS}}(\mathbf{r}) = G_{\mathbf{K}}(E, \mathbf{r})$  is a solution of the Schrödinger equation if the self-consistency relation is satisfied

$$(17) \quad U = \frac{1}{G_{\mathbf{K}}(E, 0)},$$

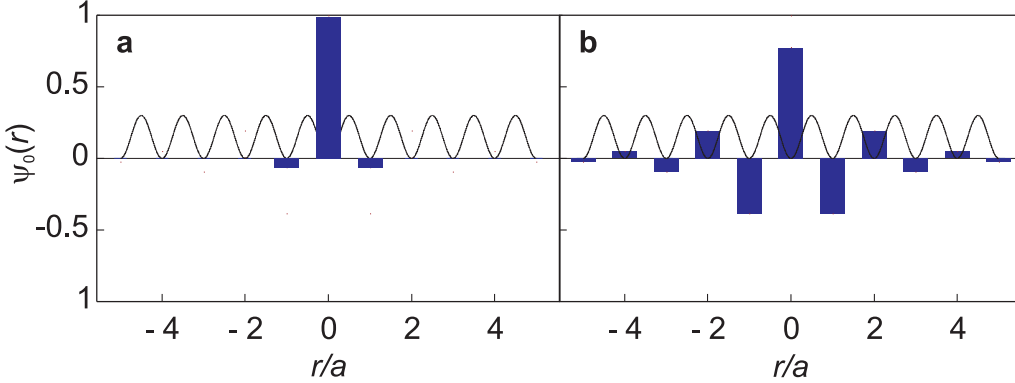


Fig. 4. – Wavefunctions  $\psi_{\mathbf{K}}(\mathbf{r})$  showing the amplitude for various site separations for repulsively bound pairs ( $a_s = 100a_0$ ) in 1D with  $K = 0$ .  $r$  denotes the separation between the two atoms. (a)  $U/J = 30$  ( $V_0 = 10E_r$ ) and (b)  $U/J = 3$  ( $V_0 = 3E_r$ ).

which determines the energy  $E_{\text{BS}}$  of the bound state  $\psi_{\mathbf{K}}^{\text{BS}}$ . The resulting bound state wavefunction,  $\psi_{\mathbf{K}}^{\text{BS}}(\mathbf{r})$  falls off exponentially for large  $r$ , and describes a bound two particle state travelling with center of mass momenta  $\mathbf{K}$  through the lattice. The momentum distribution of this bound state is then given by  $G_{\mathbf{K}}(E_{\text{BS}}, \mathbf{k})$

$$(18) \quad \psi_{\mathbf{K}}^{\text{BS}}(\mathbf{k}) = \frac{1}{E_{\text{BS}} - \epsilon_{\mathbf{K}}(\mathbf{k})}.$$

Note, that this wave function is not normalized.

In three dimensions, Eq. (17) only has a solution for interaction strengths above a critical value,  $U > U_c = -2J/G(0, 0) \approx 8J$ , and thus we require  $U > U_c$  for the formation of the bound two-particle state. The wavefunction  $\psi_{\mathbf{K}}(\mathbf{r})$  is then square-integrable, as shown in Fig.4. For a deep lattice, i.e.  $U/J \gg 1$ , bound pairs essentially consist of two atoms occupying the same site, whereas for small  $U/J$ , the pair is delocalized over several lattice sites. A main feature of the repulsive pair wavefunction is its oscillating character: the wavefunction amplitude alternates sign from one site to the next, as shown in Fig. 4. In quasimomentum space this corresponds to a wavefunction which is peaked at the edges of the first Brillouin zone, which is discussed in detail in section 6.2.

When motion is confined to one dimension the bound two particle state exists for arbitrarily small repulsive interaction  $U > 0$ , in contrast to the three-dimensional situation. Here the energy of the bound pairs, computed from Eq. (17) is  $E_{LS}(K) = 2J[\sqrt{4(\cos \frac{Ka}{2})^2 + (U/2J)^2} + 2]$ , which can be seen plotted in Fig. 3 as Bloch band of a stable composite object *above* the continuum of two particle scattering states. The figure shows how the binding energy (separation of these states from the continuum) increases as  $U/J$  is increased, and how the curvature of the band becomes less pronounced. In the limit of strong interaction,  $U \gg J$  the bound state energy reduces to

$E(K) \sim 4J + U + (4J^2/U)(1 + \cos Ka)$ , which is consistent with our expectation of a positive binding energy  $U$ , and the center of mass energy of a composite object with an effective tunnelling matrix element  $J^2/U$ .

#### 4. – Numerical approach for repulsively bound pairs

We want to be able to treat not just a single repulsively bound pair, but a lattice gas of many interacting repulsively bound pairs. This is important both in order to properly describe the effects of interactions on experimental measurements, and to investigate many-body effects on the behaviour of the pairs. Whilst perturbation theory can be used to produce useful analytical models in some limits [14], it is possible in one dimension to treat the system in more general regimes using recently developed numerical techniques.

**4.1. Time-Dependent DMRG.** – In one spatial dimension, the system of interacting repulsively bound pairs can be treated by directly simulating the Bose-Hubbard model time-dependently, using time-dependent Density Matrix Renormalisation Group (DMRG) methods [15, 16, 17, 18]. These methods allow near-exact integration of the Schrödinger equation for the 1D many body system by an adaptive decimation of the Hilbert space, provided that the resulting states can be written efficiently in the form of a truncated matrix product state (this will be explained in more detail below). This method has been successfully applied to several lattice and spin models of interest in condensed matter physics, including systems realisable using cold atoms in optical lattices [19, 20, 21, 22, 23, 24, 25]. The algorithm, both in the form originally proposed by Vidal and similar methods proposed by Verstrate and Cirac have also been generalised to the treatment of master equations for dissipative systems and systems at finite temperature [26, 27].

**4.1.1. Matrix Product States.** DMRG methods are based on a decomposition of the many-body wavefunction into a matrix product representation [18]. This requires that the original state can be expressed on a Hilbert space that is the product of local Hilbert spaces. For the Bose-Hubbard model, each local Hilbert space corresponds to a particular lattice site, and the basis states in the local Hilbert space correspond to different occupation numbers, running from 0 to  $S - 1$ . We then write the coefficients of the wavefunction expanded in terms of local Hilbert spaces of dimension  $S$ ,

$$(19) \quad |\Psi\rangle = \sum_{i_1 i_2 \dots i_M=1}^S c_{i_1 i_2 \dots i_M} |i_1\rangle \otimes |i_2\rangle \otimes \dots \otimes |i_M\rangle,$$

as a matrix product state given by

$$(20) \quad c_{i_1 i_2 \dots i_M} = \sum_{\alpha_1 \dots \alpha_{M-1}}^X \Gamma_{\alpha_1}^{[1] i_1} \lambda_{\alpha_1}^{[1]} \Gamma_{\alpha_1 \alpha_2}^{[2] i_2} \lambda_{\alpha_2}^{[2]} \Gamma_{\alpha_2 \alpha_3}^{[2] i_2} \dots \Gamma_{\alpha_{M-1}}^{[M] i_M}.$$

The  $\Gamma$  and  $\lambda$  tensors are chosen so that the tensor  $\lambda_\alpha^{[l]}$  specifies the coefficients of the Schmidt decomposition [15] for the bipartite splitting of the system at site  $l$ ,

$$(21) \quad |\psi\rangle = \sum_{\alpha=1}^{\chi_l} \lambda_\alpha^{[l]} |\phi_\alpha^{[1\dots l]}\rangle |\phi_\alpha^{[l+1\dots M]}\rangle,$$

where  $\chi_l$  is the Schmidt rank, and the sum over remaining tensors specify the Schmidt eigenstates,  $|\phi_\alpha^{[1\dots l]}\rangle$  and  $|\phi_\alpha^{[l+1\dots M]}\rangle$ . The key to the truncated matrix product state representation is that for many states corresponding to a low-energy in 1D systems we find that the Schmidt coefficients  $\lambda_\alpha^{[l]}$ , when ordered in decreasing magnitude, decay rapidly as a function of their index  $\alpha$  [15]. Thus we can truncate the representation at relatively small  $\chi$  and still provide an inner product of almost unity with the exact state of the system  $|\Psi\rangle$ . In implementations of this method we perform convergence tests for the state representation, that is, we vary the values of  $\chi$  and  $S$  to check that the point at which the representation is being truncated does not affect the final results. We also make use of an optimised version of the code in which the Schmidt eigenstates are forced to correspond to fixed numbers of particles [16, 18]. This allows us to make use of the total number conservation in the Hamiltonian to substantially increase the speed of the code, and also improve the scaling with  $\chi$  and  $S$ . With this number conserving code we are able to compute results with much higher values of  $\chi$  in a much shorter time than the original algorithm.

**4.1.2. Time Dependence.** Time dependence of these states can be computed for Hamiltonians acting only on neighbouring lattice sites because when an operator acts on the local Hilbert state of two neighbouring sites, the representation can be efficiently updated to the Matrix product state that best approximates the new state of the system. To do this, the  $\Gamma$  tensors corresponding to those two sites must be updated, a number of operations that scales as  $\chi^3 S^3$  for sufficiently large  $\chi$  [15]. In this way, we represent the state on a systematically truncated Hilbert space, which changes adaptively as we perform operations on the state. The time evolution operator  $\exp(-i\hat{H}t)$ , is then split into a product of operators, each of which acts only on a pair of neighbouring sites by means of a Suzuki-Trotter decomposition [28, 29]. This is done in small timesteps  $\delta t$ . Initial states can also be found using an imaginary time evolution, i.e., the repeated application of the operator  $\exp(-\hat{H}\delta t)$ , together with renormalisation of the state.

**4.2. Numerical Investigation of Repulsively Bound Pairs.** – In investigation of repulsively bound pairs using these methods we are able to use parameters  $U$  and  $J$  directly corresponding to values of the lattice depth  $V_0$  in the experiments, and are also able to account for the background trapping potential. We typically study 10 – 30 pairs in 60 lattice sites, and begin with an initial product state, corresponding to a random distribution of doubly-occupied and unoccupied lattice sites. We then reduce the values of  $U$  and increase the value of  $J$ , using the same time dependence for the depth of the lattice  $V_0(t)$  as in the experiment. The single particle momentum distributions can then be calculated

efficiently from the matrix product state representation, and we also average the results over different initial configurations, to match the averaging over different 1D tubes in the experiment. We can also perform lattice modulation spectroscopy, computing the time evolution of the many-body state when the parameters  $U$  and  $J$  vary as a function of time, based on the time dependence of the lattice depth  $V(t)$  used in the experiments (these calculations are similar to those in refs. [22, 25]).

## 5. – Experimental realization

In this section we describe the experimental steps to produce a pure ensemble of repulsively bound atom pairs in an optical lattice. We use  $^{87}\text{Rb}$  as the atomic species for our experiments.

**5.1. BEC production.** – We begin by creating a  $^{87}\text{Rb}$  Bose-Einstein condensate (BEC) of  $6 \times 10^5$   $^{87}\text{Rb}$  atoms in spin state  $|F = 1, m_F = -1\rangle$  in a vacuum apparatus featuring a magnetic transport line [30, 31]. This transport initially transfers laser cooled atoms from the chamber of the magneto-optical trap (MOT) into a UHV glass cell (pressure  $< 10^{-11}$  mbar) which offers good optical access from all sides. Here the BEC is produced in a QUIC trap [32, 30] with trapping frequencies  $\omega_{x,y,z} = 2\pi \times (15, 15, 150)$  Hz at a magnetic bias field of 2 G. Afterwards the QUIC trap is converted into a Ioffe-type magnetic trap with trap frequencies  $\omega_{x,y,z} = 2\pi \times (7, 19, 20)$  Hz) by adjusting the currents through the quadrupole and Ioffe coils and by applying additional magnetic field gradients. This moves the BEC over a distance of 8 mm into the center of the QUIC quadrupole coils which are later used to generate the homogeneous magnetic field for Feshbach ramping.

**5.2. Loading into lattice.** – Within 100 ms the BEC is adiabatically loaded into the vibrational ground state of an optical lattice which is  $35 E_r$  deep ( $E_r = 2\pi^2\hbar^2/m\lambda^2$ , where  $m$  is the mass of the atoms). Our 3D lattice is cubic and consists of three pairs of retro-reflected intensity-stabilized laser beams, which propagate orthogonally to each other. They are derived from a frequency-stable single-mode Ti:Sapphire laser ( $< 500$  kHz linewidth) with a wavelength of  $\lambda = 830.44$  nm. For this wavelength, the laser is detuned by about 100 GHz from the closest transition to an excited molecular level, minimizing light induced losses as a precondition for long lifetimes of pairs and molecules. The laser beams are polarized perpendicularly to each other and their frequencies differ by several tens of MHz to avoid disturbing interference effects. The waists of all three beams are about  $160 \mu\text{m}$  and the maximum obtainable power is about 110mW per beam. At this stage about 20% of the condensate atoms are grouped in pairs of two into the lattice sites. 60% of the condensate atoms are found in singly occupied sites, and another 20% percent of atoms are located in triply and more highly occupied lattice sites [33].

**5.3. Purification scheme.** – In order to remove all atoms from those lattice sites that are not occupied by exactly two atoms we use a purification scheme which involves an intermediate step in which Feshbach molecules are produced. For this, we turn off the magnetic trap and flip the spins of the  $^{87}\text{Rb}$  atoms from their initial state  $|F = 1, m_F =$

$-1\rangle$  to  $|F = 1, m_F = +1\rangle$  by suddenly reversing the bias magnetic field of a few G. This spin state features a 210 mG wide Feshbach resonance at 1007.40 G [34]. By adiabatically ramping over this resonance we convert pairs of atoms in multiply occupied lattice sites into  $\text{Rb}_2$  Feshbach molecules with almost unit efficiency [33]. After the Feshbach ramp, fast inelastic collisions will occur in sites that were initially occupied with more than two atoms. These exothermic collisions between either a created molecule and an atom or between two molecules will remove these particles from the lattice. At this stage the lattice consists only of sites which are either empty, filled with a single atom, or filled with a single Feshbach molecule. A subsequent 3ms long combined radio-frequency (rf) and optical purification pulse removes all chemically unbound atoms, thus creating a pure molecular sample of about  $2 \times 10^4$  molecules [33]. The microwave drives the transition at a frequency of 9113 MHz between levels which correlate with  $|F = 1, m_F = +1\rangle$  and  $|F = 2, m_F = +2\rangle$ . The light pulse drives the closed transition  $|F = 2, m_F = +2\rangle \rightarrow |F = 3, m_F = +3\rangle$ . The optical transition frequency is 1402 MHz blue detuned compared to the transition at zero magnetic field. The light literally blows the atoms out of the lattice, while the direct effect of the microwave and light field pulse on the molecules is negligible because the radiation is off resonance. Finally, sweeping back across the Feshbach resonance we adiabatically dissociate the dimers and obtain a lattice where  $2 \times 10^4$  sites are filled with exactly two atoms. According to section 3, at the deep lattice depth of  $35 E_r$  ( $U/J \approx 3700$ ), the corresponding two atom wavepacket matches perfectly with the wavefunction of the repulsively bound atom pair. By adiabatically lowering the lattice depth (typically within a few ms) in a horizontal direction we can then produce 1D repulsively bound atom pairs states for arbitrary values of  $U/J$ .

## 6. – Experiments

In the following we discuss the properties of the repulsively bound pairs that were experimentally investigated by measuring their lifetime, quasi-momentum distribution and binding energies. By varying the effective interaction between the atoms with the help of the Feshbach resonance we can also create lattice induced bound atom pairs which are based on attractive interactions.

**6.1. Pair lifetime.** – We have already seen from Fig. 2(right) that for a repulsive interaction with  $a_s = 100 a_0$  the lifetime of the pairs is remarkably long (700 ms, exponential fit). This lifetime is mainly limited by inelastic scattering of lattice photons [33], and greatly exceeds the calculated time for an atom to tunnel from one site to the next,  $2\pi\hbar/(4J) \sim 4$  ms. The lifetime measurements are based on lowering the lattice depth to a chosen height, and then measuring the number of remaining pairs after a variable hold time. In order to make this measurement, the lattice is adiabatically raised again to its full initial depth of  $V_0 = 35 E_r$ . Using the Feshbach resonance atoms in doubly occupied sites are converted to Feshbach molecules with near unit efficiency [33], and another combined rf-light purification pulse then removes all remaining atoms (which stem from now dissociated pairs) as in the original preparation step. Afterwards the molecules are

again converted back into atoms, and can then be detected via conventional absorption imaging.

**6.2. Quasi-momentum distribution.** – We have experimentally investigated the quasi-momentum distribution of the pairs in various regimes by mapping it onto a spatial distribution, which we measured using standard absorption imaging. For this, we first adiabatically lower the lattice depth in a horizontal direction at a rate of  $1.3 E_r/\text{ms}$  to a pre-chosen height while the lattice depth in the other two directions are kept high ( $35 E_r$ ). This will prepare repulsively bound pairs at the chosen lattice depth. We then turn off the lattice rapidly enough so that the quasi-momentum distribution cannot change, but slowly with respect to the bandgap, so that single-particle quasi-momenta are mapped to real momenta [31, 35]. We have typically employed linear ramps with rates of  $0.2 E_r/\mu\text{s}$ . The resulting momentum distribution is converted to a spatial distribution after  $\sim 15$  ms time of flight. Fig. 5 shows two measured quasi-momentum distributions for lattice depths  $V_0 = 6(20)$ , respectively. The top row shows the bare images of the atomic density taken in the laboratory. Below are the corresponding quasi-momentum distributions in horizontal direction. It is clearly visible that for low lattice depths the quasi-momentum distributions are peaked at the edges of the first Brillouin zone. For deep lattices, however, the first Brillouin zone is homogeneously filled and the quasi-momentum distribution has a flat top shape. This latter distribution is reminiscent of the one observed for a dephased ensemble of ultracold atoms in the lowest band of a lattice [31]. The agreement between experimental data and theoretical calculations is quite good. Note, however, that the experimental distributions appear to extend beyond the first Brillouin zone. This is an experimental artifact related to repulsion between atoms during expansion (before imaging) and also relatively long imaging times (many photons are scattered from each atom, which performs a random walk). This leads to smearing out of the sharp structure at the edge of the Brillouin zone. Fig. 6 shows in a more continuous fashion the dependence on lattice depth  $V_0$  of the quasi-momentum distribution for repulsively bound pairs for both experiment and numerical simulation. As discussed before, the peak structure is more pronounced for lower values of  $V_0$ , and diminishes for larger  $V_0$ . This characteristic is a clear signature of the pair wavefunction for repulsively bound pairs.

It is important to note that in all cases here we measure the distribution of single-atom quasi-momenta in a large sample. That we still obtain the peaked distribution characteristic of repulsively bound pairs is non-trivial. In fact, if we just take a single repulsively bound pair with centre of mass quasi-momentum  $K \neq 0$ , its single-atom momentum distribution will not be peaked anymore at the edges of the first Brillouin zone. The peak will be somewhat translated towards the center of the first Brillouin zone. Fortunately, with increasing  $|K|$ , the peak in the single-particle quasi-momentum distribution also becomes less pronounced. As a result, when we average over a roughly uniform distribution of centre of mass quasimomenta  $K$  for a dilute gas of repulsively bound pairs, we still observe the pronounced peaks at the edges of the Brillouin zone. This is confirmed by the numerical simulations and their good agreement with experiments.

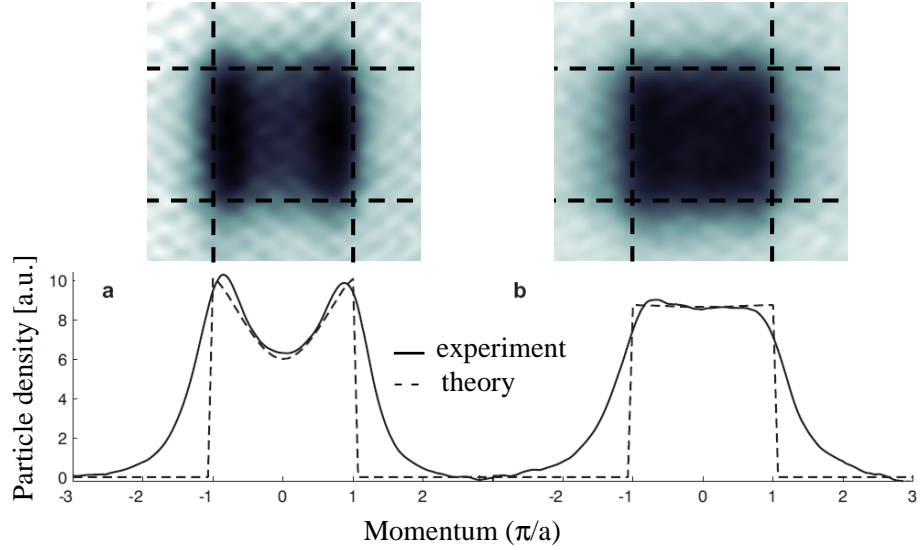


Fig. 5. – Quasi-momentum distributions of atoms in the lattice for (a)  $V_0 = 5E_R$  and (b)  $V_0 = 20E_R$ . **above** Images show absorption images of the atomic distribution after release from the 3D lattice and a subsequent 15 ms time of flight. The horizontal and vertical dashed lines enclose the first Brillouin zone. **below** Corresponding quasi-momentum distributions in the horizontal-direction, after integration over the vertical-direction. For comparison numerical simulations (see text) are also shown (dashed lines). The density values have been scaled to facilitate comparison between experimental and theoretical results.

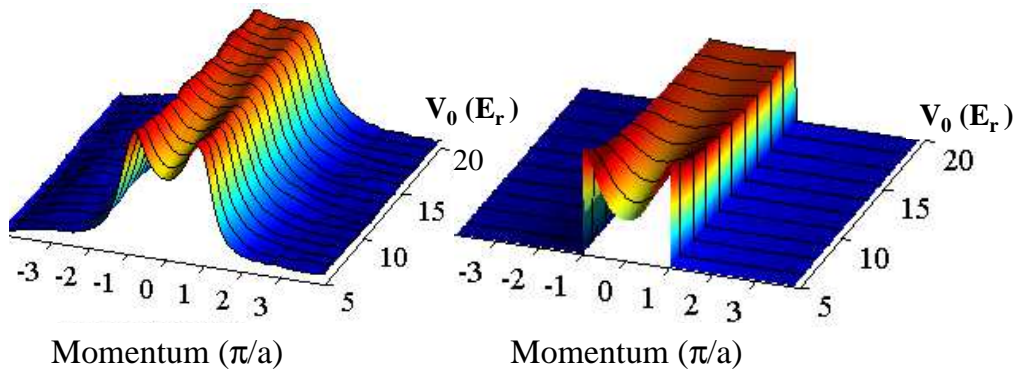


Fig. 6. – Momentum distributions similar as the ones shown in Fig.5 are plotted here as a function of lattice depth  $V_0$ . Left: experiment. Right: numerical calculation.

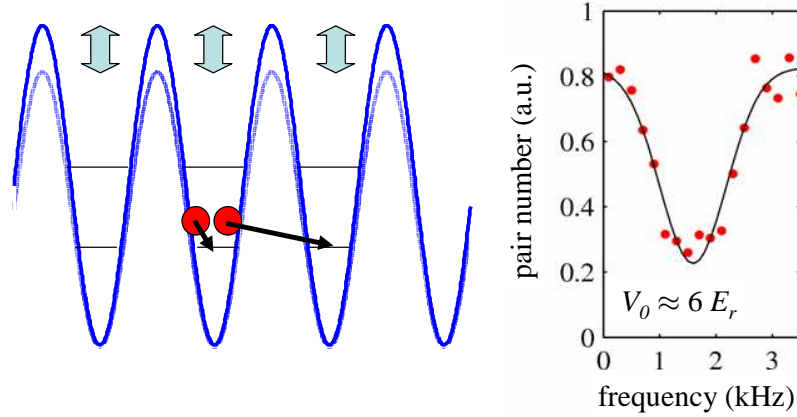


Fig. 7. – Modulation spectroscopy of repulsively bound pairs. **(left)** By modulating the optical lattice amplitude with the proper frequency, the pair can dump its binding energy into the lattice motion and subsequently break up. **(right)** Typical resonance dip showing the remaining number of atom pairs as a function of the modulation frequency, for  $V_0 \approx 6 E_r$ . The black line is a Gaussian fit, a choice which was justified by numerical calculations.

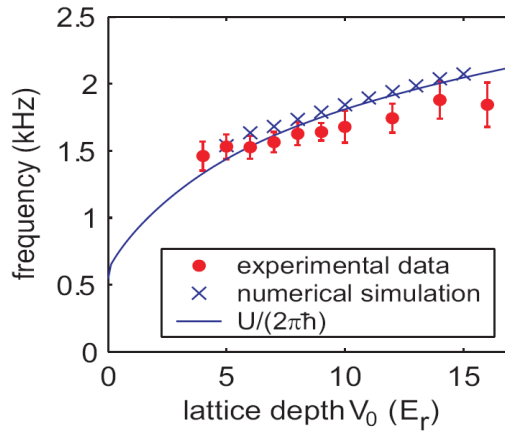


Fig. 8. – Measured resonance frequencies of the modulation spectroscopy as a function of the lattice depth. The resonance frequency was determined from resonance curves similar to the one in Fig. 7 (right). The experimental points (filled circles) show good agreement with numerical simulations (crosses) and also coincide with the onsite collisional energy shift  $U$  (line). Experimental error bars correspond to the 95% confidence interval for the Gaussian fit parameters of the resonance dips.

**6.3. Modulation spectroscopy.** – By modulating the depth of the lattice at a chosen frequency we can determine the binding energy of the pairs (see Fig. 7, left). For appropriate modulation frequencies, the pairs can dump their binding energy into the lattice motion and dissociate. Fig. 7 (right) shows a typical resonance curve of the number of remaining pairs as a function of the modulation frequency. The resonance frequency of about 1.5 kHz (for a lattice depth of  $V_0 = 6 E_r$ ) agrees well with the calculated binding energy of a pair. The width of the resonance curve can be understood, as the pair will decay into a continuum of scattering states which has an energy width of up to  $8J$  [depending on the initial centre of mass quasimomentum  $K$  (see Fig. 3)]. In addition to this width, broadening due to Fourier limited modulation pulses and inhomogeneity effects in the lattice will occur.

Modulation spectroscopy measurements were carried out for a variety of lattice depths (see Fig. 8). The resonance positions are in good agreement with numerical simulations and essentially coincide with interaction energy,  $U$ .

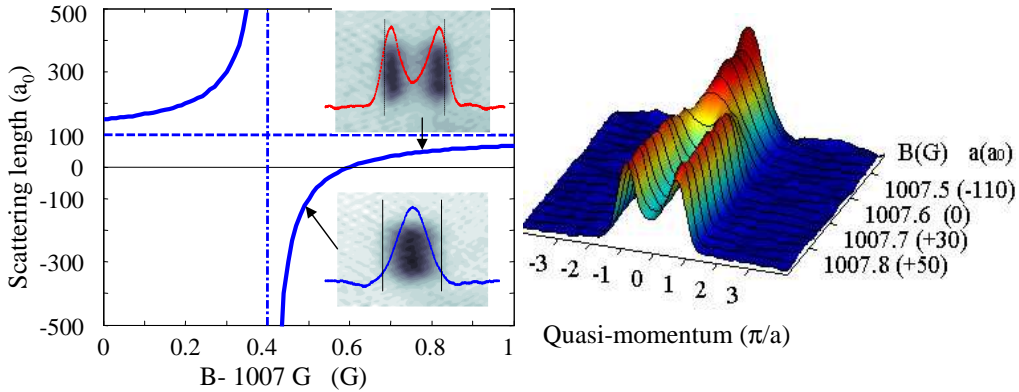


Fig. 9. – From repulsively to attractively bound atom pairs. **left** With the help of a Feshbach resonance around 1007.4 G, we can choose the effective interaction of the paired atoms by controlling the scattering length  $a$ .  $a_0$  is the Bohr radius. The inserted images show quasi-momentum distributions similar to the ones of Fig. 5. For effectively attractive interaction the quasi-momentum distribution is peaked around 0 momentum. **right** The momentum distribution for atom pairs as a function of magnetic field (scattering length.). At zero scattering length the distribution has a flat top shape. The shown data correspond to experiments where the lattice depth  $V_0$  had been adiabatically lowered in 1D below  $3E_r$ .

**6.4. Attractively bound pairs.** – Making use of the Feshbach resonance at 1007.40 G we can tune the effective interaction of the atoms within the pair (see Fig. 9, left). It is then possible to also create bound atom pairs which are based on attractive interaction. After initial production of repulsively bound atom pairs in the deep lattice ( $V_0 = 35E_r$ ), we applied an appropriate nearly homogenous magnetic offset field. This tuned the scattering length of the atomic pair from its default value of  $a_s = 100a_0$  to negative

scattering length of up to  $a_s = -110a_0$ . Afterwards the optical lattice was lowered as before. In contrast to repulsively bound pairs where the momentum distribution is peaked at the edges of the first Brillouin zone, the momentum distribution for attractively bound pairs is peaked in the center of the first Brillouin zone. This goes along with having a bound state with minimal internal energy. Fig. 9 (right) shows how the quasi-momentum distribution of the pairs changes continuously as the scattering length is changed. Interestingly, for non-interacting atoms ( $a_s = 0$ ) the distribution again becomes a flat top shape.

With respect to stability, we find that lifetimes of bound atom pairs are similar for scattering lengths of equal size but opposite sign.

## 7. – Repulsively bound pairs of fermions

Although so far we have only discussed repulsively bound pairs which are composed of *bosonic* atoms, analogous pairs can also be formed from *fermions* or *boson-fermion mixtures*. These systems will exhibit interesting physics based on their composite nature and the quantum statistics of their components.

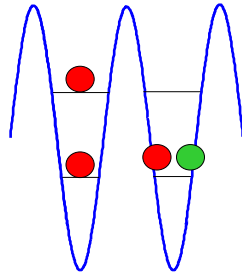


Fig. 10. – Possible realization of repulsively bound pairs with fermionic atoms. **left** In the case of two identical fermions (same spin) the atoms have to be in different bands due to the Pauli exclusion principle. **right** Fermions of different spins or Bose-Fermi mixtures, however, can occupy the same band.

Of course, in a single species fermion experiment it is not possible to put two identical fermions into the same site and band due to the Pauli exclusion principle. The two atoms would have to be at least in different bands (see Fig. 10, left), and even then the interaction between them typically would be very small in the ultracold regime.

These problems do not arise using a two-component spin mix of fermions (see Fig. 10, right), as two atoms of different spin can share the same site and band and can also interact strongly. The fact that a higher site occupancy than two is again strictly forbidden could be advantageous in the initial production of pairs. Furthermore, the pairing of two fermions can result in a pair with bosonic character. In a 3D environment pairing of fermions recently lead to interesting experiments studying the BEC-BCS transition (see

e.g. [36, 37, 38, 39, 40, 41]). It would be interesting to study similar properties to this transition with repulsive pairing, investigating the system as the interaction strength is changed.

Also it would be very interesting to study repulsive pairs which are a composite objects of a fermion and a boson. One question would be how these bound states, would interact with each other, and how, for example, the bosonic atoms within the pair would mediate next neighbor interactions [11].

## 8. – Other related physical systems

Although no stable repulsively bound pairs have previously been observed, their physics is partially related to other physical systems. Here we briefly discuss a few examples of such systems with bound states which are in a way reminiscent of repulsively bound states.

**8.1. Pairing resonances in many-body systems.** – For example, resonance behaviour based on similar pairing of Fermions of different spin in the Hubbard model was first discussed by Yang [42], and plays an important role in SO(5) theories of superconductivity [43]. There are several examples of many-body bound states that can occur for repulsive as well as attractive interactions, such as the resonances discussed in the context of the Hubbard model by Demler et al. [44]. Such resonance behaviour is common in many-body physics, although states of this type are normally very short-lived. Optical lattice experiments will now provide an opportunity to prepare and investigate stable versions of such states, which until now have only appeared virtually as part of complex processes.

**8.2. Excitons.** – The stability and many-body physics of repulsively bound pairs is perhaps most closely associated with that of excitons, which are *attractively* bound pairs of a particle in the conduction band and a hole in the valence band of a periodic system [45]. These bind to form a composite boson, a gas of which can, in principle, Bose-condense. Excitons are excited states of the many-body system, but are bound by an attractive interaction between the particle and hole that form the pair. They are also discussed in the specific context of fermionic systems. However, a single exciton on a lattice could have a description very similar to that of a single repulsively bound pair, and could be realised and probed in optical lattices experiments [46].

**8.3. Photonic crystals.** – Repulsively bound atom pairs in an optical lattice are also reminiscent of photons being trapped by impurities in photonic crystals [47], which consist of transparent material with periodically changing index of refraction. An impurity in that crystal in the form of a local region with a different index of refraction can then give rise to a localized field eigenmode. In an analogous sense, each atom in a repulsively bound pair could be seen as an impurity that “traps” the other atom.

**8.4. Gap solitons.** – An analogy can also be drawn between repulsively bound atom pairs and gap solitons, especially as found in atomic gases [48, 49, 50, 51]. Solitons

are normally a non-linear wave phenomenon, and in this sense have a very different behaviour to repulsively bound pairs, which exhibit properties characteristic of many-body quantum systems. However, there has been increasing recent interest in discussing the limit of solitons in atomic systems where very few atoms are present, giving rise to objects that are often referred to as quantum solitons [52, 53, 54]. These are N-body bound states in 1D, and thus a 2-atom bright quantum soliton is a bound state of two atoms moving in 1D. In this sense, the solution for a single repulsively bound pair in 1D is related to a single quantum soliton on a lattice.

## 9. – Conclusion

We have reviewed theoretically and experimentally the physics of repulsively bound pairs of atoms in an optical lattice. The good agreement between experiment and theory exemplifies the strong correspondence between the optical lattice physics of ultra-cold atoms and the Hubbard model on a new level, a connection which has particular importance for applications of these cold atom systems to more general simulation of condensed matter models and to quantum computing. The existence of such metastable bound objects will be ubiquitous in cold atoms lattice physics, giving rise to new potential composite objects also in fermions or in systems with mixed Bose-Fermi statistics. These states could also be formed with more than two particles, or as bound states of existing composite particles. Repulsively bound pairs have no direct counterpart in condensed matter physics due to the strong inelastic decay channels observed in solid state lattices, and could be a building block of yet unstudied quantum many body states or phases.

\* \* \*

We would like to thank our fellow team members who contributed to the research work on repulsively bound atom pairs: Hanspeter Büchler, Rudi Grimm, Adrian Kantian, Florian Lang, Gregor Thalhammer, Klaus Winkler, and Peter Zoller. We would like to thank Eugene Demler for interesting discussions. We acknowledge support from the Austrian Science Fund (FWF) within the Spezialforschungsbereich 15, from the European Union within the OLAQUI and SCALA networks, from the TMR network "Cold Molecules", and the Tiroler Zukunftsstiftung.

## REFERENCES

- [1] JAKSCH D. and ZOLLER P., *Annals of Physics*, **315** (2005) 52 and references therein.
- [2] BLOCH I., *Nature Physics*, **1** (2005) 23.
- [3] GREINER M., MANDEL O., ESSLINGER T., HÄNSCH T. W. and BLOCH I., *Nature*, **415** (2002) 39.
- [4] PAREDES B., WIDERA A., MURG V., MANDEL O., FÖLLING S., CIRAC I., SHLYAPNIKOV G. V., HÄNSCH T.W., and BLOCH I., *Nature*, **429** (2004) 277.
- [5] STÖFERLE T., MORITZ H., SCHORI C., KÖHL M. and ESSLINGER T., *Phys. Rev. Lett.*, **92** (2004) 130403.

- [6] KINOSHITA T., WENGER T. and WEISS, D. S., *Science*, **305** (2004) 1125.
- [7] LABURTHE TOLRA B., O'HARA K. M., HUCKANS J. H., PHILLIPS W. D., ROLSTON S. L. and PORTO J. V., *Phys. Rev. Lett.*, **92** (2004) 190401.
- [8] FALLANI L., LYE J. E., GUARRERA V., FORT C. and INGUSCIO M., cond-mat/0603655 (2006).
- [9] WINKLER K., THALHAMMER G., LANG F., GRIMM R., HECKER DENSCHLAG J., DALEY A. J., A. KANTIAN A., BÜCHLER H. P. and ZOLLER P., *Nature*, **441** (2006) 853.
- [10] HOFSTETTER W., CIRAC J. I., ZOLLER P., DEMLER E. and LUKIN M. D., *Phys. Rev. Lett.*, **89** (2002) 220407.
- [11] LEWENSTEIN M., SANTOS L., BARANOV M. A. and FEHRMANN H., *Phys. Rev. Lett.*, **92** (2004) 050401.
- [12] FISHER M. P. A., WEICHMAN P. B., GRINSTEIN G., and FISHER D. S., *Phys. Rev. B*, **40** (1989) 546.
- [13] CSERTI J., *American Journal of Physics*, **68** (2000) 896.
- [14] PETROSYAN D., FLEISCHHAUER M., ANGLIN J. R., cond-mat/0610198.
- [15] VIDAL G., *Phys. Rev. Lett.*, **91** (2003) 147902; **93** (2004) 040502.
- [16] DALEY A. J., KOLLATH C., SCHOLLWÖCK U. and VIDAL G., *J. Stat. Mech.: Theory Exp.*, **P04005** (2004) .
- [17] WHITE S. R. and FEIGUIN A. E., *Phys. Rev. Lett.*, **93** (2004) 076401.
- [18] SCHOLLWÖCK U., *Rev. Mod. Phys.*, **77** (2005) 259.
- [19] GOBERT D., KOLLATH C., SCHOLLWÖCK U. and SCHÜTZ G., *Phys. Rev. E*, **71** (2005) 036102.
- [20] DALEY A. J., CLARK S. R., JAKSCH D. and ZOLLER P., *Phys. Rev. A*, **72** (2005) 043618.
- [21] KOLLATH C., SCHOLLWÖCK U., and ZWERGER W., *Phys. Rev. Lett.*, **95** (2005) 176401.
- [22] KOLLATH C., IUCCI A., GIAMARCHI T., HOFSTETTER W. and SCHOLLWÖCK U., *Phys. Rev. Lett.*, **97** (2006) 050402.
- [23] CLARK S. R. and JAKSCH D., *Phys. Rev. A*, **70** (2004) 043612.
- [24] AL-HASSANIEH K. A., FEIGUIN A. E., RIERA J. A. , BUSSE C. A. and DAGOTTO E., cond-mat/0601411.
- [25] KOLLATH C., IUCCI A., MCCULLOCH I. and GIAMARCHI T., cond-mat/0608091.
- [26] ZWOLAK M. and VIDAL G., *Phys. Rev. Lett.*, **93** (2004) 207205.
- [27] VERSTRAETE F., GARCIA-RIPOLL J. J. and CIRAC J. I., *Phys. Rev. Lett.*, **93** (2004) 207204.
- [28] SUZUKI M., *Phys. Lett. A*, **146** (1990) 6.
- [29] SUZUKI M., *J. Math. Phys.*, **32** (1991) 2.
- [30] THALHAMMER G., THEIS M., WINKLER K., GRIMM R. and HECKER DENSCHLAG J., *Phys. Rev. A*, **71** (2005) 033403.
- [31] GREINER M., BLOCH I., HÄNSCH T. W., and ESSLINGER T., *Phys. Rev. A*, **63** (2001) 031401(R).
- [32] ESSLINGER T., BLOCH I., and HÄNSCH T. W., *Phys. Rev. A*, **58** (1998) 2664(R).
- [33] THALHAMMER G., WINKLER K., LANG F., SCHMID S., GRIMM R. and HECKER DENSCHLAG J., *Phys. Rev. Lett.*, **96** (2006) 050402.
- [34] VOLZ T., DÜRR S., ERNST S., MARTE A. and REMPE, G., *Phys. Rev. A*, **68** (2003) 010702.
- [35] HECKER DENSCHLAG J., SIMSARIAN J. E., HÄFFNER H., MCKENZIE C., BROWAEYS A., CHO D., HELMERSON K., ROLSTON S. L., and PHILLIPS W. D., *J. Phys. B*, **35** (2002) 3095.
- [36] REGAL C. A., GREINER M. and JIN D. S., *Phys. Rev. Lett.*, **92** (2004) 040403.
- [37] CHIN C., BARTENSTEIN M., ALTMAYER A., RIEDL S., JOCHIM S., HECKER DENSCHLAG J. and GRIMM R., *Science*, **305** (2004) 1128.

- [38] KINAST J., HEMMER S. L., GEHM M. E., TURLAPOV A., and THOMAS J. E., *Phys. Rev. Lett.*, **92** (2004) 150402.
- [39] BOURDEL T., KHAYKOVICH L., CUBIZOLLES J., ZHANG J., CHEVY F., TEICHMANN M., TARRUELL L., KOKKELMANS S. J. J. M. F. and C. SALOMON, *Phys. Rev. Lett.*, **93** (2004) 050401.
- [40] ZWIERLEIN M. W., ABO-SHAER J. R., SCHIROTZEK A., SCHUNCK C. H., and KETTERLE W., *Nature*, **435** (2005) 1047.
- [41] PARTRIDGE G. B., STRECKER K. E., KAMAR R. I., JACK M. W., and HULET R. G., *Phys. Rev. Lett.*, **95** (2005) 020404.
- [42] YANG C.N., *Phys. Rev. Lett.*, **63** (1989) 2144.
- [43] DEMLER E., HANKE W. and ZHANG S. C., *Rev. Mod. Phys.*, **76** (2004) 909.
- [44] DEMLER E. and ZHANG S. C., *Phys. Rev. Lett.*, **75** (1995) 4126.
- [45] MOSKALENKO S. A. and SNOKE D. W., *Bose-Einstein Condensation of Excitons and Biexcitons* (Cambridge University Press, Cambridge, 2000).
- [46] KANTIAN A. ET AL., in preparation.
- [47] JOANNOPOULOS J. D., MEADE R. D. and WINN J. N., *Photonic Crystals: Molding the Flow of Light*, Princeton University Press, Princeton, 1995.
- [48] LOUIS P. J. Y., OSTROVSKAYA E. A., SAVAGE C. M. and KIVSHAR YU. S., *Phys. Rev. A*, **67** (2003) 013602.
- [49] EFREMIDIS N. K. and CHRISTODOULIDES D. N., *Phys. Rev. A*, **67** (2003) 063608.
- [50] EIERMANN B., ANKER TH., ALBIEZ M., TAGLIEBER M., TREUTLEIN P., MARZLIN K. P. and OBERTHALER M. K., *Phys. Rev. Lett.*, **92** (2004) 230401.
- [51] AHUFINGER V., SANPERA A., PEDRI P., SANTOS L. and LEWENSTEIN M., *Phys. Rev. A*, **69** (2004) 053604.
- [52] DRUMMOND P. D., KHERUNTSYAN K. V. and HE H., *J. Opt. B: Quant. Semiclass. Optics*, **1** (1999) 387.
- [53] BULLOUGH R. K. and WADATI M., *J. Opt. B: Quant. Semiclass. Optics*, **6** (2004) S205.
- [54] MAZETS I. E. and KURIZKI G., *Eur. Phys. Lett.*, **76** (2006) 196.